Towards On-Demand Heralded Single-Photon Sources via Photon Blockade

Jiangshan Tang,[1,2] Lei Tang,[1] Haodong Wu,[1] Yang Wu,[1,3] Hui Sun,[3,*] Han Zhang,[1,2,†] Tao Li,[4] Yanqing Lu (陆延青),[1,2] Min Xiao,[1,2,5] and Keyu Xia (夏可宇)[1,2,‡]

[1] *College of Engineering and Applied Sciences, National Laboratory of Solid State Microstructures, and Collaborative Innovation Center of Advanced Microstructures, Nanjing University, Nanjing 210023, China*

[2] *School of Physics, Nanjing University, Nanjing 210023, China*

[3] *School of Physics and Information Technology, Shaanxi Normal University, Xi'an 710062, China*

[4] *School of Science, Nanjing University of Science and Technology, Nanjing 210094, China*

[5] *Department of Physics, University of Arkansas, Fayetteville, Arkansas 72701, USA*

Spontaneous parametric down-conversion (SPDC) in a laser pumped optical nonlinear medium can produce heralded single photons with a high purity but a very low yield. Improving the yield by increasing the pump power in SPDC inevitably reduces the purity due to excitation of multiphoton events. We propose a scheme to overcome this purity-yield trade-off by suppressing multiphoton events in a cavity-enhanced SPDC via the photon-blockade effect. By introducing a strong photon-photon interaction into the intracavity medium and increasing the pump power, we can improve the available single-photon yield to larger than 90%, while keeping the purity high, towards on-demand generation of single photons through the SPDC process. Our quasi-on-demand SPDC sources may boost single-photon-based quantum-information technology.

I. INTRODUCTION

Single photons are at the heart of photon-based quantum-information processing [1–3], such as quantum communication [4], quantum simulations [5], and linear optical quantum computing [6]. The quality of single-photon sources directly determines the development and performance of photon-based quantum-information technology [7–10].

Various methods have been studied for generating single photons, including photon blockade of a weak coherent field [11,12], nonlinear wave mixing [13,14], and cavity quantum electrodynamics (CQED) [15–19]. Among these methods, CQED systems using quantum dots (QDs) have achieved great success in generating single photons [17–20]. Some advanced techniques such as the dichromatic excitation [21] and asymmetrical cavities are reported to overcome the challenging issues of polarization filtering [19], and spectral overlap with the exciting laser [22].

Another widely used approach of generating single photons is the heralded single-photon source (HSPS) based on spontaneous parametric down-conversion (SPDC) in

an optical nonlinear medium. Because a HSPS can work at room temperature, significantly simplifying the requirement of implementation, it provides one of the leading platforms for many applications in quantum-information technologies, in particular, requiring a narrow-band photon source [23–28]. HSPSs are almost perfect in all aspects such as indistinguishability [18], high purity [2], flexibility [27], and scalability [29], except for the only drawback of the small photon yield, which is typically few parts per thousand for guaranteeing a high purity [2]. Cavity-enhanced narrow-band SPDC can reduce the single-photon bandwidth to fit atomic systems and quantum memory [23,25], which normally operates in megahertz to gigahertz and at room temperature [30].

There is a trade-off between the purity and the yield per pump pulse, namely the purity-yield limitation, in HSPSs [2,31,32]. To produce heralded single photons with a high single-photon purity, the pump laser in the conventional HSPS must be weak enough that the probability of multiphoton emissions is negligibly small. Inevitably, a weak pumping also leads to a small generation probability of single photons, i.e., low single-photon yield. This inherent constraint between high single-photon purity and large photon yield is the fundamental limitation of applications of HSPSs [4,33]. It is worth noting that multiplexed HSPS can improve the single-photon yield of signal mode without considerably reducing the purity by

* physsunh@snnu.edu

† zhanghan@nju.edu.cn

‡ keyu.xia@nju.edu.cn

detecting an idler photon from many individual HSPSs, or with different spectral components or time bin of a single photon generated in successive SPDC processes [34–38]. However, overcoming the purity-yield trade-off still remains a challenge. A principle breakthrough of solving this inherent limitation is the key to boosting applications of HSPSs, even opening up unprecedented single-photon-based quantum-information technologies.

In this paper, we propose a scheme to improve the single-photon generation efficiency, namely yield per pump pulse, of HSPS based on the cavity-enhanced SPDC but keep a high purity, therefore overcoming the purity-yield limitation.

II. SYSTEM AND MODEL

Our system overcoming the purity-yield trade-off in cavity-enhanced HSPS via the photon blockade is depicted in Fig. 1(a). A pump laser beam with frequency ω_p and effective pump power $\xi\sqrt{P}$ is input into the ring optical cavity formed with reflective mirrors M1–M4. It drives a type-II phase-matched periodically poled KTiOPO$_4$ (PPKTP) crystal to induce an optical SPDC process [25]. This SPDC process emits photons in pairs: the idler and signal modes a_i and a_s with frequency ω_i and ω_s, respectively, doubly resonant with the cavity [39–41]. The counterpropagating cavity modes are decoupled from the SPDC due to the chirality in frequency conversion. The idler mode is orthogonal in polarization to and different in frequency from the signal mode. It is off resonance with atomic transitions and thus decouples from rubidium (Rb) atoms. The pump laser is separated by the dichroic mirror from the generated photons. The idler photon outputting
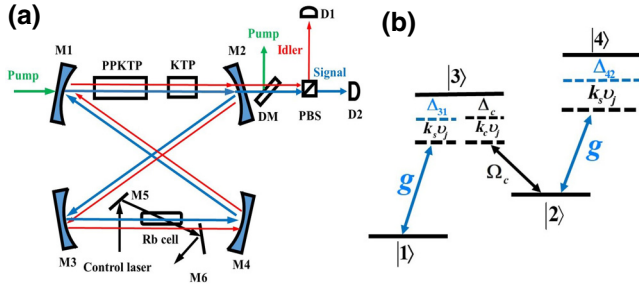

FIG. 1. (a) Schematic setup for overcoming the purity-yield trade-off in HSPS. A pump laser enters the ring cavity and drives a PPKTP crystal to produce idler-signal photon pairs. A KTP crystal enables dual-mode resonance for the idler and signal modes. The control laser is used to induce strong PPI in warm atoms for the signal mode. M1–M6, mirrors; DM, dichroic mirror; PBS, polarization beam splitter; D1 and D2, single-photon detectors. (b) Level diagram of N-type atoms. The signal photon (control field) drives the transitions $|1\rangle \leftrightarrow |3\rangle$ and $|2\rangle \leftrightarrow |4\rangle$ ($|2\rangle \leftrightarrow |3\rangle$) with detuning Δ_{31} and Δ_{42} (Δ_c), and corresponding coupling strength g (Ω_c).

from M2 is reflected by the PBS to the idler output channel and monitored by a single-photon detector D1. The signal mode couples to Rb atoms and is subject to a strong photon-photon interaction (PPI) induced by the control laser field [42]. It is then detected by another detector D2.

The N-type Rb atoms embedded in the optical cavity at room temperature creates a large PPI for the signal mode under the driving of the control laser [42]. The energy levels of the N-type atom are denoted as $|l\rangle$ with eigenfrequency ω_l ($l = 1, 2, 3, 4$), as shown in Fig. 1(b). The state $|3\rangle$ decays to the states $|1\rangle$ and $|2\rangle$ with rates γ_{31} and γ_{32}, respectively. The state $|4\rangle$ decays at a rate γ_{42}. The dephasing rates of both ground states $|1\rangle$ and $|2\rangle$ are γ_{21}. For simplicity, we assume $\gamma_{31} = \gamma_{32} = \gamma_{42} = \gamma_0$ and $\gamma_{21} \ll \gamma_0$ for Rb atoms [9,43,44]. The cavity mode couples to the transitions $|1\rangle \leftrightarrow |3\rangle$ and $|2\rangle \leftrightarrow |4\rangle$ with strength g. The control laser beam has an angular frequency ω_c, and drives the transition $|2\rangle \leftrightarrow |3\rangle$ with Rabi frequency Ω_c. In the rotating frame, defined by an unitary transformation $U_1 = \exp\{i\sum_{j=1}^{N}[\omega_1\sigma_{11}^j + (\omega_s + \omega_1 - \omega_c)\sigma_{22}^j + (\omega_s + \omega_1)\sigma_{33}^j + (2\omega_s + \omega_1 - \omega_c)\sigma_{44}^j]t + i(\omega_i a_i^\dagger a_i + \omega_s a_s^\dagger a_s)t\}$, the Hamiltonian of the system takes the form ($\hbar = 1$) $H = \sum_{j=1}^{N}\sum_{l=2}^{4}\Delta_{ll}\sigma_{ll}^j + \xi\sqrt{P}(e^{-i\Delta_p t}a_i^\dagger a_s^\dagger + e^{i\Delta_p t}a_i a_s) + \sum_{j=1}^{N}\left[g(a_s^\dagger\sigma_{13}^j + a_s^\dagger\sigma_{24}^j) + \Omega_c\sigma_{23}^j + \text{h.c.}\right]$ [45], with $\Delta_{22} = \Delta_c - \Delta_{31}$, $\Delta_{33} = -\Delta_{31}$, $\Delta_{44} = \Delta_c - \Delta_{42} - \Delta_{31}$, and $\Delta_p = \omega_p - \omega_s - \omega_i$. $\sigma_{mn}^j = |m\rangle\langle n|$ ($m, n = 1, 2, 3, 4$) denotes the transition operator for the jth atom. $\Delta_{31} = \omega_s - \omega_{31}$ ($\Delta_{42} = \omega_s - \omega_{42}$) is the detuning between the cavity mode and the transition of $|3\rangle \leftrightarrow |1\rangle$ ($|4\rangle \leftrightarrow |2\rangle$), and $\Delta_c = \omega_c - \omega_{32}$ is the detuning between the control field and the $|3\rangle \leftrightarrow |2\rangle$ transition ($\omega_{mn} = \omega_m - \omega_n$). Only the signal mode in the cavity interacts with atoms. At room temperature, the inevitable random thermal motion of the jth atom moving with velocity v_j causes the "microscopic" Doppler shifts $k_s v_j$ and $k_c v_j$, corresponding to wave vectors k_s and k_c of the cavity and control fields, respectively. Here we have $|k_s| \approx |k_c|$ and approximately take both as k. The control and the cavity fields propagate in the same direction that $k_s v_j \approx k_c v_j$ [9]. We consider the condition of $|g| \ll |\Omega_c|$, leading to the population of the atomic ground state $\rho_{11} \approx 1$. Then we use the perturbation approach to solve the master equation and obtain the effective PPI coefficient in the presence of thermal motion as [9,42,46–49]

$$\eta = \int \frac{ig^4\gamma_{32}}{|\Omega_c|^4\gamma_{21}(\gamma_{31} + \gamma_{32})}\left(\frac{1}{F(v)} + \frac{1}{F^*(v)}\right)$$
$$\times \left[\frac{(2\gamma_{21} + \gamma_{32})}{\gamma_{32}}\left(\frac{1}{F^*(v)} - \frac{1}{F(v)}\right)\right.$$
$$\left. + \left(\frac{1}{F_1(v)} - \frac{1}{F_1^*(v)}\right)\right]N(v)dv, \tag{1}$$

where $F = -1/(i\Delta_{22} + \gamma_{21}/2) - [i(\Delta_{31} + kv) + (\gamma_{31} + \gamma_{32})/2]/|\Omega_c|^2$, $F_1 = 1/[-i(\Delta_{42} - \Delta_c) - (\gamma_{42} + \gamma_{31} + \gamma_{32})/2] - [i(\Delta_{42} + kv) + (\gamma_{21} + \gamma_{42})/2]/|\Omega_c|^2$. The atomic velocity has the Maxwell-Boltzmann distribution that $N(v) = N_a e^{-v^2/u^2}/u\sqrt{\pi}$, where u is the room-mean-square atomic velocity, and N_a is the total atom number. At room temperature, $ku \approx 300$ MHz for Rb atoms [50]. This Kerr nonlinearity causes the PPI. This perturbation approach provides an estimation of Kerr nonlinearity in good agreement with experimental observations [42–44,51–54]. Moreover, the Kerr nonlinearity can be enhanced by increasing the number of atoms or adjusting Ω_c.

Applying a unitary transformation of $U_2 = \exp\{i(\omega_p - \omega_i - \omega_s)a_s^\dagger a_s t\}$ to the system, we get the effective Hamiltonian

$$H_{\text{eff}} = (\Delta - \eta - \Delta_p)a_s^\dagger a_s + \eta(a_s^\dagger a_s)^2 + \xi\sqrt{P}(a_i^\dagger a_s^\dagger + a_i a_s), \tag{2}$$

where $\Delta = \int N(v)dv((g^2/\Omega_c^2)\{\gamma_{32}(\Delta_{31} - \Delta_c)/[\gamma_{21}(\gamma_{31} + \gamma_{32})](1/F + 1/F^*) + [\Delta_{31} + kv)/(\gamma_{31} + \gamma_{32})](1/F + 1/F^*) + i(1/F^* - 1/F)\})$. The influence of the unwanted linear frequency shift Δ can be eliminated by selecting an appropriate pump frequency ω_p that $\Delta = \Delta_p$. The PPI causes an energy shift $\eta(a_s^\dagger a_s)^2$ to the cavity mode a_s. This energy shift depends on the cavity excitation $\langle a_s^\dagger a_s \rangle$. Once the cavity mode is excited to include a on-resonance signal photon ($\Delta_p = \Delta$), exciting a second signal photon in the cavity requires additional 2η energy and is suppressed. This photon-blockade effect can be used to suppress multiphoton events in the SPDC.

The master equation of the density matrix ρ describing the dynamics of our system is given by $\dot{\rho}(t) = -i[H_{\text{eff}}, \rho(t)] + \mathcal{L}\{\kappa_i, a_i\}\rho + \mathcal{L}\{\kappa_s, a_s\}\rho$, where $\kappa_i = \kappa_{i,ex} + \kappa_{i,\text{in}}$ ($\kappa_s = \kappa_{s,\text{ex}} + \kappa_{s,\text{in}}$) is the decay rate of the idler (signal) mode. The subscripts "ex" and "in" indicate the external rate and the internal loss rate, respectively. We assume $\kappa_{i,\text{ex}} = \kappa_{s,\text{ex}} = \kappa_{\text{ex}}$ and $\kappa_{i,\text{in}} = \kappa_{s,\text{in}} = \kappa_{\text{in}}$. The Lindblad term is $\mathcal{L}\{\kappa_l, a_l\}\rho = \kappa_l\left[2a_l\rho(t)a_l^\dagger - a_l^\dagger a_l\rho(t) - \rho(t)a_l^\dagger a_l\right]$ with $l \in \{i, s\}$. Using the density matrix, we can evaluate the photon states in the cavity. In experiment, the photons escape from the cavity after the pump pulse is switched off and then are detected.

We do an ensemble of quantum trajectory simulation for calculating the population of each photonic state in the outgoing wave functions by counting the collapse of the system state over a period $\kappa_s t = 6$ [12,49,55–57]. This period allows the generated photons to completely escape from the cavity.

The escape efficiency of signal (idler) photons is evaluated as $\eta_{\text{esc},s(i)} = \kappa_{\text{ex}}/(\kappa_{\text{ex}} + \kappa_{\text{in}})$ [58]. Unlike the waveguide-based HSPS with a large mode mismatching [59]. the axial symmetric cavity-mode profile in our HSPS

can match the geometry of output mirror well. The cavity internal loss can be small [59] and the escape efficiency approaches to unity [39,60,61]. To focus on the key physics of interest, we consider the ideal case $\eta_{\text{esc},s(i)} = 1$.

The purity of the HSPS can be evaluated through the equal time second-order autocorrelation function $g_s^{(2)}(0)$ of the signal mode, conditional on the detection of the idler photon [2]. In our setup, once an idler photon is detected by D1, the system state degrades to a reduced density matrix ρ_s. The autocorrelation function $g_s^{(2)}(0)$ is given by [49,62–64]

$$g_s^{(2)}(0) = \frac{\langle a_s^\dagger(t)a_s^\dagger(t)a_s(t)a_s(t)\rangle_i}{\langle a_s^\dagger(t)a_s(t)\rangle_i^2} = \frac{\sum_{n_s \geq 1} n_s(n_s - 1)\alpha_{n_s}}{(\sum_{n_s} n_s\alpha_{n_s})^2}, \tag{3}$$

where $\langle\cdots\rangle_i$ is the average over the postmeasurement state when an idler photon is measured. $\alpha_{n_s} = \sum_{n_i>0} P_{n_s,n_i}/\sum_{n_s',n_i'>0} P_{n_s',n_i'}$ is the n-signal-photon probability after detecting an idler photon. P_{n_s,n_i} is the probability of the states $|n_s, n_i\rangle$ under the Fock states' representation of the associating system of the idler and signal modes. The output signal mode is antibunching if $g_s^{(2)}(0) < 1$.

In conventional HSPSs, improving the photon yield by increasing the pump laser power can cause reduction of the single-photon purity. This inherent but critical issue fundamentally limits scaling up of HSPS-based applications [2,37]. We show a strong photon blockade can effectively suppress the generation of multiphoton pairs and thus guarantees a high purity but allows us to greatly improve the photon yield by increasing the pump laser power.

Below is the physical mechanism breaking the purity-yield limitation. When the signal mode is excited in the nonlinear cavity, excitation of high Fock states is blocked due to the photon-blockade effect. In the SPDC process, the idler and signal photons are always generated in pairs. Therefore, if the signal mode can only be generated in the form of single photon, the idler mode is also subject to the same situation. As a result, the generation of the high Fock-state photon pairs $|n_s, n_i\rangle$ ($n_s = n_i \geq 2$) is also blocked. On the other hand, the probability of generating single-photon pairs becomes larger because the pump laser power is stronger. In this way, we fundamentally circumvent the inherent contradiction between remaining high purity and improving yield of HSPSs.

III. FIXED-DURATION PULSE EXCITATION

A. Single-photon yield per pump pulse

The evolution of the system can be obtained by solving the master equation. The probability of generating a single photon in each outgoing light pulse is a good measure of the yield Y per pump pulse or brightness [2]. If P_n is the n-photon number probability, then $Y = P_1$ for $P_1 \gg P_{n>1}$

and $Y = 1$ for a deterministic single-photon source [2]. In our system, as signal photons and idler photons are created in pairs, then $Y = P_{11}$. For convenience, here the subscripts in P_{n_s,n_i} represent signal and idler photon numbers, respectively. Note that the yield Y is essentially different from the so-called single-photon heralding efficiency. The later describes the probability of successfully heralding a signal photon when an idler photon is detected [61,65]. Even at a low yield of photon pair $|11\rangle$, high heralding efficiency can be obtained [26,62].

Figure 2(a) shows the population P_{11} of single-photon pair state $|1, 1\rangle$ versus the pump laser power $\xi\sqrt{P}$ and the PPI strength η. The duration τ_p of the pump laser pulse is fixed at $\tau_p = \pi/40\kappa_s$. When $\eta \gg \kappa_s$, the population P_{11} can be significantly improved and peaks when $2\xi\sqrt{P}\tau_p = \pi$, corresponding to a π pump pulse. For $\eta/\kappa_s > 75$ and $15 < \xi\sqrt{P}/\kappa_s < 25$, see the white solid curve, the yield can be higher than 80%. A larger PPI allows us to achieve $Y > 90\%$, see the red dashed curve. For a given PPI strength η, the population P_{11} shows a cosinelike oscillation as $\xi\sqrt{P}$ increases. Two reasons cause this behavior: one is the excitation population oscillations as the pump pulse area $2\xi\sqrt{P}\tau_p$ increases, and the other is that the given PPI becomes not large enough to suppress the multiphoton pair generation excited by a strong pump field.

The available maximum yield is determined by the pump power $\xi\sqrt{P}$ and the PPI strength η, see Fig. 2(b). Enhancing the pump power can improve the single-photon yield, and increasing the PPI can suppress the multiphoton excitation. Without nonlinearity-induced photon blockade, the probability of creating photon pairs $|n_s, n_i\rangle$ scales with pump intensity to the nth power as predicted theoretically [2,49], see Fig. 2(b). The maximum yield can only be 23.8% at $\xi\sqrt{P}/\kappa_s \simeq 11$ at the expense of low purity ($\Pi \approx 4.3\%$) due to high excitation of multiphoton-pair states [31]. With photon blockade, multiphoton events almost disappear, see the curves for P_{22} and P_{33} in Fig. 2(b). When $\eta/\kappa_s = 80$, we obtain the maximum probability P_{11}, i.e., the yield, of 81% at $\xi\sqrt{P}/\kappa_s \simeq 19$. Meanwhile, the vacuum state population drops rapidly with the pump power.
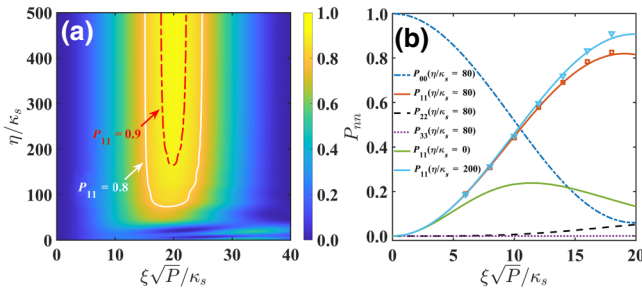
We can further improve the yield to 0.9 for $\eta/\kappa_s = 200$ and $\xi\sqrt{P}/\kappa_s = 19$. When the yield is higher than 90%, it is reasonable to claim that the HSPS becomes quasi-on-demand [66]. By "quasi-on-demand," we mean each pump pulse can generate a single-photon pulse with a large probability [67].

B. Single-photon purity

The single-photon purity Π can be characterized by the second-order autocorrelation function $g_s^{(2)}(0)$ [2,19,49,68]. For a high purity, we use the relation $\Pi \approx 1 - g_s^{(2)}(0)$ [17,49]. Figure 3(a) shows the correlation function $g_s^{(2)}(0)$ versus the PPI strength and the pump power. We obtain a high purity $\Pi > 90\%$ when η is large enough, see the white solid curve. In the overlap region marked by the curves showing $P_{11} > 0.8$ and $g_s^{(2)}(0) < 0.1$, we simultaneously obtain $Y > 80\%$ and $\Pi > 90\%$. A larger pump power leads to a decrease in the purity, because the probability of multiphoton events becomes higher as the pump power increases, see P_{22} and P_{33} in Fig. 2(b). In contrast to conventional HSPSs, increasing the PPI strength in our scheme can suppress the excitation of multiphoton states, and maintain the high purity.

In Fig. 3(b), we show the equal time second-order autocorrelation function $g_s^{(2)}(0)$ as an indicator of the single-photon purity for different PPI strengths. When the PPI is absent or small, $g_s^{(2)}(0)$ increases to larger than unity as the pump power increases, corresponding to the case of heralded single-photon generation under a strong pumping. Without the PPI, we derive $g_s^{(2)}(0) \approx 2\tanh^2(\xi\sqrt{P}\tau_p)$ [49], in good agreement with the numerical result. The purity-yield product is always bounded by 0.09. The difference at high pump power is due to the truncation of Hilbert space in simulation [49]. The purity increases rapidly as the PPI becomes larger. For example, when $\eta/\kappa_s = 80$, the yield is already 80% and the purity reaches 91% [$g_s^{(2)}(0) = 0.09$] at $\xi\sqrt{P}/\kappa_s = 17$. If $\eta/\kappa_s = 200$, the yield and the purity increase to 91% and 99%, respectively.
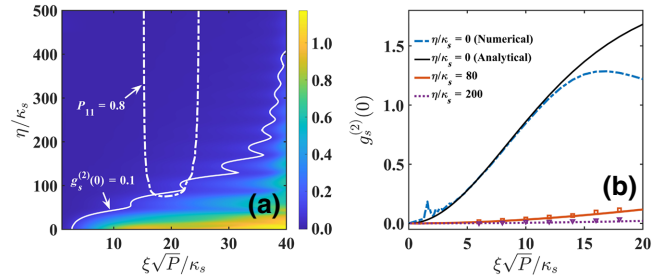

FIG. 2. (a) Population P_{11} versus $\xi\sqrt{P}$ and η. (b) Population of paired Fock states $|n_s, n_i\rangle$ as a function of $\xi\sqrt{P}$ with different PPI strength. Other parameters are $\kappa_s = \kappa_i = 1$ and $\tau_p = \pi/40\kappa_s$.

FIG. 3. (a) The equal-time second-order autocorrelation $g_s^{(2)}(0)$ versus $\xi\sqrt{P}$ and η. (b) The second-order autocorrelation $g_s^{(2)}(0)$ as a function of $\xi\sqrt{P}$ with different PPI strength η. Other parameters are $\kappa_s = \kappa_i = 1$ and $\tau_p = \pi/40\kappa_s$.

IV. π-PULSE EXCITATION

In our scheme, high Fock states of signal and idler modes are suppressed due to the photon-blockade effect. To provide an apparent physical picture, we truncate the photonic basis to include only the vacuum and single-photon pair states in the cavity. In the effective two-state space, the state $|1,1\rangle$ can be completely populated from the vacuum state with a π pump pulse [17,49]. In a real case including high Fock-state photon pairs, instead of fixing the pump pulse duration τ_p but changing the pump power $\xi\sqrt{P}$, we fix the pump pulse area $2\xi\sqrt{P}\tau_p = \pi$ to excite the single-photon pair $|1,1\rangle$ and investigate the influence of the pump power on the yield and purity of HSPS. As shown in Fig. 4, the single-photon yield can increase to 80% at $\xi\sqrt{P}/\kappa_s = 6.6$ under π-pulse excitation, in comparison with a yield of 22.6% in fix-duration excitation. At the same time, the purity remains nearly unchanged, larger than 99% in both excitation cases. For relative low pump power, the yield under π-pulse excitation (dashed curves) is much higher than the case of fix-duration excitation corresponding to a small pulse area (solid curves). In contrast, the purities in both cases are very close. Thus, a π pulse can excite the single-photon pair state more efficiently and a high purity is guaranteed by the photon-blockade effect. When η is large enough, the nonlinear cavity can be modeled as a two-level system [69]. Then, our HSPS is equivalent to a CQED-based single-photon source. Thus, the yield can approach unity in theory. To show this, we calculate the yield and the purity in a very large PPI regime. For example, when $\eta/\kappa_s = 500$, we obtain $Y = 95\%$ and $\Pi \approx 99\%$ ($g^{(0)} \approx 0.01$) at $\xi\sqrt{P}/\kappa_s = 40$.

The generated photons are detected after escaping from the cavity. The quantum-statistical characters of single-photon pairs outside the cavity is close to those in the cavity when the pump laser is switched off, see the
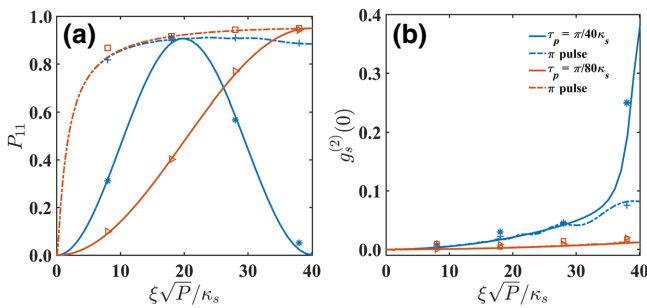

FIG. 4. Population of Fock state $|1,1\rangle$ (a) and the second-order autocorrelation $g_s^{(2)}$ (b) versus the pump power $\xi\sqrt{P}$. Blue (red) solid curves indicate the case with a fixed pulse duration $\tau_p = \pi/40\kappa_s$ and the PPI strength $\eta/\kappa_s = 200$ ($\tau_p = \pi/80\kappa_s$ and $\eta/\kappa_s = 500$). Blue (red) dash-dotted curves represent the results for π-pulse excitation, i.e., $2\xi\sqrt{P}\tau_p = \pi$, in the case of $\eta/\kappa_s = 200$ ($\eta/\kappa_s = 500$). Other parameters are $\kappa_s = \kappa_i = 1$.

quantum trajectory simulation data markers at $\xi\sqrt{P}/\kappa_s = \{6, 8, 10, 12, 14, 16, 18\}$ in Figs. 2(b) and 3(b), and at $\xi\sqrt{P}/\kappa_s = \{8, 18, 28, 38\}$ in Fig. 4.

V. IMPLEMENTATION

Our scheme can be implemented with a setup of a four-mirror ring cavity [70–72], as depicted in Fig. 1(a). The mirror M2 has a relatively low reflectivity (87.5%) as the output port [39]. The other three mirrors have high reflectivity of 99.99% [73]. End faces of the PPKTP and KTP crystals and the atomic cell are coated with 99.9% antireflection layers for both the idler and signal modes. We use the 0.8-m-long ring cavity. The cavity internal losses is calculated to be $\kappa_{\rm in} = 2\pi \times 0.37$ MHz and the external loss rate is $\kappa_{\rm ex} = 2\pi \times 8$ MHz, yielding $\kappa_s = 2\pi \times 8.37$ MHz. The escape efficiency can reach $\eta_{\rm esc,s(i)} = 95.6\%$. Warm Rb atoms with $\gamma_0 = 2\pi \times 6$ MHz [9] are used to create a strong PPI for the signal mode a_s. Four levels related to the D1 line of ^{87}Rb atom in the N-type configuration are $|1\rangle = |5^2S_{1/2}, F = 1, m_F = -1\rangle$, $|2\rangle = |5^2S_{1/2}, F = 2, m_F = 0\rangle$, $|3\rangle = |5^2P_{1/2}, F' = 2, m'_F = -1\rangle$ and $|4\rangle = |5^2P_{1/2}, F' = 2, m'_F = 0\rangle$. The signal mode and control laser drive the corresponding transitions in Fig. 1(b) with detunings $\Delta_{31} = 18\kappa_s \approx 904$ MHz, $\Delta_c = 0$, and $\Delta_{42} = 8.5\Delta_{31}$. We obtain $\eta/\kappa_s = 200$ when $\Omega_c = 30\gamma_0$ (0.9 mW [74]) and $N_a(g/\kappa_s)^4 \sim 2.3 \times 10^3$. With a π excitation, we obtain $Y = 0.9$, $\Pi = 99\%$ and $\eta_{\rm esc,s}\eta_{\rm esc,i} = 91.4\%$, yielding a generation rate of 1.2 MHz, when the total period of single-photon pulses takes $6\kappa_s^{-1}$. Alternatively, we can also use the N-type configuration in Ref. [42] to achieve the same strong PPI [49].

HSPSs and the SPDC process have been realized in on-chip microring resonators [27,28]. Atomic cladding photonic circuits have also been reported recently [75–77]. Therefore, our scheme has the potential to be integrated on a chip if the microring resonator is cladded by Rb atoms. In such an on-chip realization, the PPI can be significantly increased because the atom-light interaction in a microring resonator is much stronger. We can expect better performance of our HSPS.

VI. CONCLUSION

By exploiting the photon blockade in the cavity-enhanced HSPS, we solve the challenging problem of simultaneously achieving high purity and high yield in HSPSs. Our HSPS may open a door for scalable photon-based quantum-information processing.

––––––––––––

[1] Pieter Kok, W. J. Munro, Kae Nemoto, T. C. Ralph, Jonathan P. Dowling, and G. J. Milburn, Linear optical quantum computing with photonic qubits, Rev. Mod. Phys. **79**, 135 (2007).

[2] Pascale Senellart, Glenn Solomon, and Andrew White, High-performance semiconductor quantum-dot single-photon sources, Nat. Nanotechnol. **12**, 1026 (2017).

[3] C. L. Degen, F. Reinhard, and P. Cappellaro, Quantum sensing, Rev. Mod. Phys. **89**, 035002 (2017).

[4] Jian-Wei Pan, Zeng-Bing Chen, Chao-Yang Lu, Harald Weinfurter, Anton Zeilinger, and Marek Żukowski, Multiphoton entanglement and interferometry, Rev. Mod. Phys. **84**, 777 (2012).

[5] I. M. Georgescu, S. Ashhab, and Franco Nori, Quantum simulation, Rev. Mod. Phys. **86**, 153 (2014).

[6] Han-Sen Zhong, *et al.*, Quantum computational advantage using photons, Science, **370**, eabe8770 (2020).

[7] Peter Lodahl, Sahand Mahmoodian, and Søren Stobbe, Interfacing single photons and single quantum dots with photonic nanostructures, Rev. Mod. Phys. **87**, 347 (2015).

[8] Han-Sen Zhong, *et al.*, 12-Photon Entanglement and Scalable Scattershot Boson Sampling with Optimal Entangled-Photon Pairs from Parametric Down-Conversion, Phys. Rev. Lett. **121**, 250505 (2018).

[9] Keyu Xia, Franco Nori, and Min Xiao, Cavity-Free Optical Isolators and Circulators Using a Chiral Cross-Kerr Nonlinearity, Phys. Rev. Lett. **121**, 203602 (2018).

[10] Lin Li, Zexuan Liu, Xifeng Ren, Shuming Wang, Vin-Cent Su, Mu-Ku Chen, Cheng Hung Chu, Hsin Yu Kuo, Biheng Liu, Wenbo Zang, Guangcan Guo, Lijian Zhang, Zhenlin Wang, Shining Zhu, and Din Ping Tsai, Metalens-array-based high-dimensional and multiphoton quantum source, Science **368**, 1487 (2020).

[11] A. Imamoḡlu, H. Schmidt, G. Woods, and M. Deutsch, Strongly Interacting Photons in a Nonlinear Cavity, Phys. Rev. Lett. **79**, 1467 (1997).

[12] Ao Li, Tian Chen, Yiheng Zhou, and Xiangbin Wang, On-demand single-photon sources via quantum blockade and applications in decoy-state quantum key distribution, Opt. Lett. **41**, 1921 (2016).

[13] Chun-Hua Yuan, L. Q. Chen, Z. Y. Ou, and Weiping Zhang, Generation of frequency-multiplexed entangled single photons assisted by entanglement, Phys. Rev. A **83**, 054302 (2011).

[14] J. W. Silverstone, D. Bonneau, K. Ohira, N. Suzuki, H. Yoshida, N. Iizuka, M. Ezaki, C. M. Natarajan, M. G. Tanner, R. H. Hadfield, V. Zwiller, G. D. Marshall, J. G. Rarity, J. L. O'Brien, and M. G. Thompson, On-chip quantum interference between silicon photon-pair sources, Nat. Photonics **8**, 104 (2014).

[15] A. A. Houck, D. I. Schuster, J. M. Gambetta, J. A. Schreier, B. R. Johnson, J. M. Chow, L. Frunzio, J. Majer, M. H. Devoret, S. M. Girvin, and R. J. Schoelkopf, Generating single microwave photons in a circuit, Nature (London) **449**, 328 (2007).

[16] C. Lang, C. Eichler, L. Steffen, J. M. Fink, M. J. Woolley, A. Blais, and A. Wallraff, Correlations, indistinguishability and entanglement in Hong-Ou-Mandel experiments at microwave frequencies, Nat. Phys. **9**, 345 (2013).

[17] Xing Ding, Yu He, Z.-C. Duan, Niels Gregersen, M.-C. Chen, S. Unsleber, S. Maier, Christian Schneider, Martin Kamp, Sven Höfling, Chao-Yang Lu, and Jian-Wei Pan, On-Demand Single Photons with High Extraction Efficiency and Near-Unity Indistinguishability from a Resonantly Driven Quantum Dot in a Micropillar, Phys. Rev. Lett. **116**, 020401 (2016).

[18] N. Somaschi, V. Giesz, L. De Santis, J. C. Loredo, M. P. Almeida, G. Hornecker, S. L. Portalupi, T. Grange, C. Antón, J. Demory, C. Gómez, I. Sagnes, N. D. Lanzillotti-Kimura, A. Lemaítre, A. Auffeves, A. G. White, L. Lanco, and P. Senellart, Near-optimal single-photon sources in the solid state, Nat. Photonics **10**, 340 (2016).

[19] Hui Wang, *et al.*, Towards optimal single-photon sources from polarized microcavities, Nat. Photonics **13**, 770 (2019).

[20] Yanjun Bao, Qiaoling Lin, Rongbin Su, Zhang-Kai Zhou, Jindong Song, Juntao Li, and Xue-Hua Wang, On-demand spin-state manipulation of single-photon emission from quantum dot integrated with metasurface, Sci. Adv. **6**, eaba8761 (2020).

[21] Yu-Ming He, Hui Wang, Can Wang, M. C. Chen, Xing Ding, Jian Qin, Z. C. Duan, Si Chen, J. P. Li, Run-Ze Liu, C. Schneider, Mete Atatüre, Sven Höfling, Chao-Yang Lu, and Jian-Wei Pan, Coherently driving a single quantum two-level system with dichromatic laser pulses, Nat. Phys. **15**, 941 (2019).

[22] Z. X. Koong, E. Scerri, M. Rambach, M. Cygorek, M. Brotons-Gisbert, R. Picard, Y. Ma, S. I. Park, J. D. Song, E. M. Gauger, and B. D. Gerardot, Coherent Dynamics in Quantum Emitters Under Dichromatic Excitation, Phys. Rev. Lett. **126**, 047403 (2021).

[23] Z. Y. Ou and Y. J. Lu, Cavity Enhanced Spontaneous Parametric Down-Conversion for the Prolongation of Correlation Time Between Conjugate Photons, Phys. Rev. Lett. **83**, 2556 (1999).

[24] P. G. Evans, R. S. Bennink, W. P. Grice, T. S. Humble, and J. Schaake, Bright Source of Spectrally Uncorrelated Polarization-Entangled Photons with Nearly Single-Mode Emission, Phys. Rev. Lett. **105**, 253601 (2010).

[25] Han Zhang, Xian-Min Jin, Jian Yang, Han-Ning Dai, Sheng-Jun Yang, Tian-Ming Zhao, Jun Rui, Yu He, Xiao Jiang, Fan Yang, Ge-Sheng Pan, Zhen-Sheng Yuan, You-jin Deng, Zeng-Bing Chen, Xiao-Hui Bao, Shuai Chen, Bo Zhao, and Jian-Wei Pan, Preparation and storage of frequency-uncorrelated entangled photons from cavity-enhanced spontaneous parametric downconversion, Nat. Photonics **5**, 628 (2011).

[26] Sergei Slussarenko, Morgan M. Weston, Helen M. Chrzanowski, Lynden K. Shalm, Varun B. Verma, Sae Woo Nam, and Geoff J. Pryde, Unconditional violation of

the shot-noise limit in photonic quantum metrology, Nat. Photonics **11**, 700 (2017).

[27] Xiang Guo, Chang-ling Zou, Carsten Schuck, Hojoong Jung, Risheng Cheng, and Hong X. Tang, Parametric downconversion photon-pair source on a nanophotonic chip, Light: Sci. Appl. **6**, e16249 (2017).

[28] Zhaohui Ma, Jia-Yang Chen, Zhan Li, Chao Tang, Yong Meng Sua, Heng Fan, and Yu-Ping Huang, Ultrabright Quantum Photon Sources on Chip, Phys. Rev. Lett. **125**, 263602 (2020).

[29] M. J. Collins, C. Xiong, I. H. Rey, T. D. Vo, J. He, S. Shahnia, C. Reardon, T. F. Krauss, M. J. Steel, A. S. Clark, and B. J. Eggleton, Integrated spatial multiplexing of heralded single-photon sources, Nat. Commun. **4**, 2582 (2013).

[30] K. F. Reim, J. Nunn, V. O. Lorenz, B. J. Sussman, K. C. Lee, N. K. Langford, D. Jaksch, and I. A. Walmsley, Towards high-speed optical quantum memories, Nat. Photonics **4**, 218 (2010).

[31] Andreas Christ and Christine Silberhorn, Limits on the deterministic creation of pure single-photon states using parametric down-conversion, Phys. Rev. A **85**, 023829 (2012).

[32] Masahiro Takeoka, Rui-Bo Jin, and Masahide Sasaki, Full analysis of multi-photon pair effects in spontaneous parametric down conversion based photonic quantum information processing, New J. Phys. **17**, 043030 (2015).

[33] Thomas Jennewein, Marco Barbieri, and Andrew G. White, Single-photon device requirements for operating linear optics quantum computing outside the post-selection basis, J. Mod. Opt. **58**, 276 (2011).

[34] A. L. Migdall, D. Branning, and S. Castelletto, Tailoring single-photon and multiphoton probabilities of a single-photon on-demand source, Phys. Rev. A **66**, 053805 (2002).

[35] T. B. Pittman, B. C. Jacobs, and J. D. Franson, Single photons on pseudodemand from stored parametric downconversion, Phys. Rev. A **66**, 042303 (2002).

[36] M. Grimau Puigibert, G. H. Aguilar, Q. Zhou, F. Marsili, M. D. Shaw, V. B. Verma, S. W. Nam, D. Oblak, and W. Tittel, Heralded Single Photons Based on Spectral Multiplexing and Feed-Forward Control, Phys. Rev. Lett. **119**, 083601 (2017).

[37] F. Kaneda and P. G. Kwiat, High-efficiency single-photon generation via large-scale active time multiplexing, Sci. Adv. **5**, eaaw8586 (2019).

[38] Hao Yu, Chenzhi Yuan, Ruiming Zhang, Zichang Zhang, Hao Li, You Wang, Guangwei Deng, Lixing You, Haizhi Song, Zhiming Wang, Guang-Can Guo, and Qiang Zhou, Spectrally multiplexed heralded single photon source at telecom-band, arXiv:2104.02593 (2021).

[39] J. S. Neergaard-Nielsen, B. Melholt Nielsen, H. Takahashi, A. I. Vistnes, and E. S. Polzik, High purity bright single photon source, Opt. Express **15**, 7940 (2007).

[40] Xiao-Hui Bao, Yong Qian, Jian Yang, Han Zhang, Zeng-Bing Chen, Tao Yang, and Jian-Wei Pan, Generation of Narrow-Band Polarization-Entangled Photon Pairs for Atomic Quantum Memories, Phys. Rev. Lett. **101**, 190501 (2008).

[41] Han-Ning Dai, Han Zhang, Sheng-Jun Yang, Tian-Ming Zhao, Jun Rui, You-Jin Deng, Li Li, Nai-Le Liu, Shuai Chen, Xiao-Hui Bao, Xian-Min Jin, Bo Zhao, and Jian-Wei

Pan, Holographic Storage of Biphoton Entanglement, Phys. Rev. Lett. **108**, 210501 (2012).

[42] Jiteng Sheng, Xihua Yang, Haibin Wu, and Min Xiao, Modified self-Kerr-nonlinearity in a four-level N-type atomic system, Phys. Rev. A **84**, 053820 (2011).

[43] Zi-Yu Liu, Yi-Hsin Chen, Yen-Chun Chen, Hsiang-Yu Lo, Pin-Ju Tsai, Ite A. Yu, Ying-Cheng Chen, and Yong-Fan Chen, Large Cross-Phase Modulations at the Few-Photon Level, Phys. Rev. Lett. **117**, 203601 (2016).

[44] Steven Sagona-Stophel, Reihaneh Shahrokhshahi, Bertus Jordaan, Mehdi Namazi, and Eden Figueroa, Conditional π-Phase Shift of Single-Photon-Level Pulses at Room Temperature, Phys. Rev. Lett. **125**, 243601 (2020).

[45] Nicolas Sangouard, Christoph Simon, Hugues de Riedmatten, and Nicolas Gisin, Quantum repeaters based on atomic ensembles and linear optics, Rev. Mod. Phys. **83**, 33 (2011).

[46] Jiangshan Tang, Yang Wu, Zhenkai Wang, Hui Sun, Lei Tang, Han Zhang, Tao Li, Yanqin Lu, Min Xiao, and Keyu Xia, Vacuum-induced surface-acoustic-wave phonon blockade, Phys. Rev. A **101**, 053802 (2020).

[47] Marlan O. Scully, M. Suhail Zubairy, *et al.*, *Quantum Optics* (Cambridge University Press, Cambridge, 1997).

[48] Katsunari Okamoto, *Fundamentals of Optical Waveguides* (Academic Press, New York, 2006).

[49] See Supplemental Material at http://link.aps.org/supplemental/10.1103/PhysRevApplied.15.064020 for the derivation of the PPI strength, the zero-delay second-order correlation function, nonblockade case, the discussion of the effects of nonpaired photon states, decay rate of cavity modes, and quantum trajectory simulation of the output photons.

[50] Haibin Wu, J. Gea-Banacloche, and Min Xiao, Observation of Intracavity Electromagnetically Induced Transparency and Polariton Resonances in a Doppler-Broadened Medium, Phys. Rev. Lett. **100**, 173602 (2008).

[51] Hai Wang, David Goorskey, and Min Xiao, Enhanced Kerr Nonlinearity via Atomic Coherence in a Three-Level Atomic System, Phys. Rev. Lett. **87**, 073601 (2001).

[52] Shujing Li, Xudong Yang, Xuemin Cao, Chunhong Zhang, Changde Xie, and Hai Wang, Enhanced Cross-Phase Modulation Based on a Double Electromagnetically Induced Transparency in a Four-Level Tripod Atomic System, Phys. Rev. Lett. **101**, 073602 (2008).

[53] Yanhua Wang, Jinyin Wan, Bichen Zou, Jiepeng Zhang, and Yifu Zhu, Coherent manipulation of quantum states in a coupled cavity-atom system, J. Phys.: Conf. Ser. **414**, 012001 (2013).

[54] En-Ze Li, Dong-Sheng Ding, Yi-Chen Yu, Ming-Xin Dong, Lei Zeng, Wei-Hang Zhang, Ying-Hao Ye, Huai-Zhi Wu, Zhi-Han Zhu, Wei Gao, Guang-Can Guo, and Bao-Sen Shi, Experimental demonstration of cavity-free optical isolators and optical circulators, Phys. Rev. Res. **2**, 033517 (2020).

[55] M. B. Plenio and P. L. Knight, The quantum-jump approach to dissipative dynamics in quantum optics, Rev. Mod. Phys. **70**, 101 (1998).

[56] Sébastien Gleyzes, Stefan Kuhr, Christine Guerlin, Julien Bernu, Samuel Deléglise, Ulrich Busk Hoff, Michel Brune, Jean-Michel Raimond, and Serge Haroche, Quantum jumps of light recording the birth and death of a photon in a cavity, Nature (London) **446**, 297 (2007).

[57] J. R. Johansson, P. D. Nation, and Franco Nori, Qutip: An open-source python framework for the dynamics of open quantum systems, Comput. Phys. Commun. **183,** 1760 (2012).

[58] O. Morin, M. Körber, S. Langenfeld, and G. Rempe, Deterministic Shaping and Reshaping of Single-Photon Temporal Wave Functions, Phys. Rev. Lett. **123,** 133602 (2019).

[59] Kai-Hong Luo, Harald Herrmann, Stephan Krapick, Benjamin Brecht, Raimund Ricken, Viktor Quiring, Hubertus Suche, Wolfgang Sohler, and Christine Silberhorn, Direct generation of genuine single-longitudinal-mode narrowband photon pairs, New J. Phys. **17,** 073039 (2015).

[60] F. Wolfgramm, X. Xing, A. Cerè, A. Predojević, A. M. Steinberg, and M. W. Mitchell, Bright filter-free source of indistinguishable photon pairs, Opt. Express **16,** 18145 (2008).

[61] H. Le Jeannic, V. B. Verma, A. Cavailles, F. Marsili, M. D. Shaw, K. Huang, O. Morin, S. W. Nam, and J. Laurat, High-efficiency WSi superconducting nanowire single-photon detectors for quantum state engineering in the near infrared, Opt. Lett. **41,** 5341 (2016).

[62] Sylvain Fasel, Olivier Alibart, Sébastien Tanzilli, Pascal Baldi, Alexios Beveratos, Nicolas Gisin, and Hugo Zbinden, High-quality asynchronous heralded single-photon source at telecom wavelength, New J. Phys. **6,** 163 (2004).

[63] Matthias Scholz, Lars Koch, and Oliver Benson, Statistics of Narrow-Band Single Photons for Quantum Memories Generated by Ultrabright Cavity-Enhanced Parametric Down-Conversion, Phys. Rev. Lett. **102,** 063603 (2009).

[64] E. Bocquillon, C. Couteau, M. Razavi, R. Laflamme, and G. Weihs, Coherence measures for heralded single-photon sources, Phys. Rev. A **79,** 035801 (2009).

[65] Jiamin Li, Jie Su, Liang Cui, Tianqi Xie, Z. Y. Ou, and Xiaoying Li, Generation of pure-state single photons with high heralding efficiency by using a three-stage nonlinear interferometer, Appl. Phys. Lett. **116,** 204002 (2020).

[66] Natasha Tomm, Alisa Javadi, Nadia Olympia Antoniadis, Daniel Najer, Matthias Christian Löbl, Alexander Rolf Korsch, Rüdiger Schott, Sascha René Valentin, Andreas Dirk Wieck, Arne Ludwig, and Richard John Warburton, A bright and fast source of coherent single photons, Nat. Nanotechnol. **16,** 399 (2021).

[67] M. D. Eisaman, J. Fan, A. Migdall, and S. V. Polyakov, Invited review article: Single-photon sources and detectors, Rev. Sci. Instrum. **82,** 071101 (2011).

[68] Kevin A. Fischer, Lukas Hanschke, Jakob Wierzbowski, Tobias Simmet, Constantin Dory, Jonathan J. Finley, Jelena Vučković, and Kai Müller, Signatures of two-photon pulses from a quantum two-level system, Nat. Phys. **13,** 649 (2017).

[69] Zhiguang Yan, Yu-Ran Zhang, Ming Gong, Yulin Wu, Yarui Zheng, Shaowei Li, Can Wang, Futian Liang, Jin Lin, Yu Xu, Cheng Guo, Lihua Sun, Cheng-Zhi Peng, Keyu Xia, Hui Deng, Hao Rong, J. Q. You, Franco Nori, Heng Fan, Xiaobo Zhu, and Jian-Wei Pan, Strongly correlated quantum walks with a 12-qubit superconducting processor, Science **364,** 753 (2019).

[70] Min Xiao, Yong-qing Li, Shao-zheng Jin, and Julio Gea-Banacloche, Measurement of Dispersive Properties of Electromagnetically Induced Transparency in Rubidium Atoms, Phys. Rev. Lett. **74,** 666 (1995).

[71] N. Lilienfein, C. Hofer, S. Holzberger, C. Matzer, P. Zimmermann, M. Trubetskov, V. Pervak, and I. Pupeza, Enhancement cavities for few-cycle pulses, Opt. Lett. **42,** 271 (2017).

[72] Shicheng Zhang, Yiqi Hu, Gongwei Lin, Yueping Niu, Keyu Xia, Jiangbin Gong, and Shangqing Gong, Thermal-motion-induced non-reciprocal quantum optical system, Nat. Photonics **12,** 744 (2018).

[73] Andreas Muller, Edward B. Flagg, John R. Lawall, and Glenn S. Solomon, Ultrahigh-finesse, low-mode-volume fabry-perot microcavity, Opt. Lett. **35,** 2293 (2010).

[74] Hao Zhang, Limei Wang, Jie Chen, Shanxia Bao, Linjie Zhang, Jianming Zhao, and Suotang Jia, Autler-townes splitting of a cascade system in ultracold cesium Rydberg atoms, Phys. Rev. A **87,** 033835 (2013).

[75] L. Stern, B. Desiatov, I. Goykhman, and U. Levy, Nanoscale light-matter interactions in atomic cladding waveguides, Nat. Commun. **4,** 1548 (2013).

[76] Ralf Ritter, Nico Gruhler, Wolfram Pernice, Harald Kübler, Tilman Pfau, and Robert Löw, Atomic vapor spectroscopy in integrated photonic structures, Appl. Phys. Lett. **107,** 041101 (2015).

[77] Ralf Ritter, Nico Gruhler, Helge Dobbertin, Harald Kübler, Stefan Scheel, Wolfram Pernice, Tilman Pfau, and Robert Löw, Coupling Thermal Atomic Vapor to Slot Waveguides, Phys. Rev. X **8,** 021032 (2018).